A COMPARISON OF MEASURED AND CALCULATED ACOUSTIC REFLECTION COEFFICIENTS FOR A SATURATED KAOLIN-WATER ARTIFICIAL SEDIMENT

Robert Morgan Wellborn

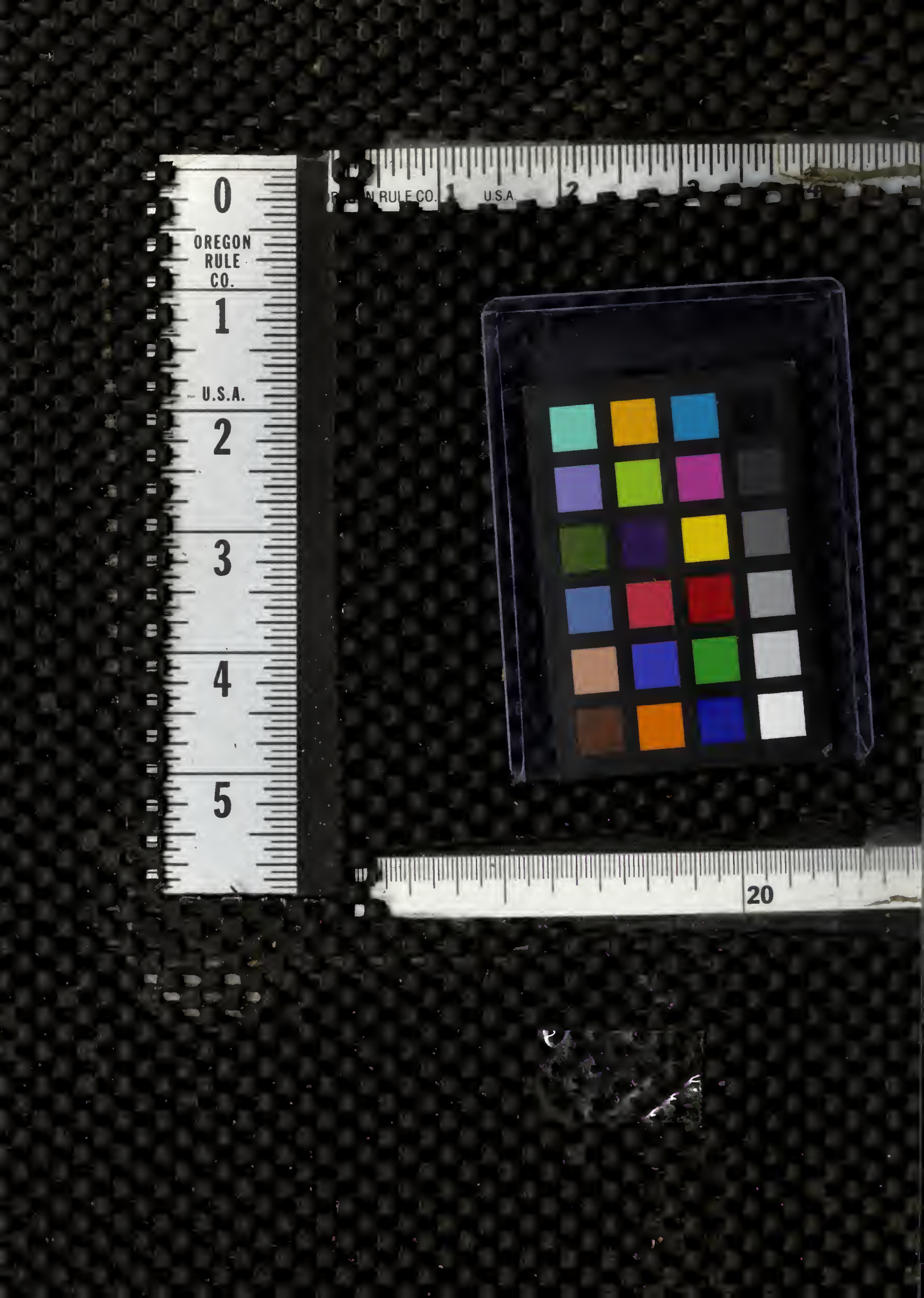
0
OREGON
RULE
CO.
1
U.S.A.
2
3
4
5
U.S.A.
20

A COMPARISON OF MEASURED AND CALCULATED ACOUSTIC REFLECTION COEFFICIENTS FOR A SATURATED KAOLIN-WATER ARTIFICIAL SEDIMENT

Robert Morgan Wellborn

NAVAL POSTGRADUATE SCHOOL
Monterey, California

THESIS

A COMPARISON OF MEASURED AND CALCULATED ACOUSTIC REFLECTION COEFFICIENTS FOR A SATURATED KAOLIN-WATER ARTIFICIAL SEDIMENT

by

Robert Morgan Wellborn, Jr.

Thesis Advisor: O. B. Wilson, Jr.

December 1973

Approved for public release; distribution unlimited.

A Comparison of Measured and Calculated Acoustic Reflection Coefficients for a Saturated Kaolin-Water Artificial Sediment

by

Robert Morgan Wellborn, Jr.
Commander, United States Navy
B.S., United States Naval Academy, 1957

Submitted in partial fulfillment of the
requirements for the degree of

MASTER OF SCIENCE IN ENGINEERING ACOUSTICS

from the

NAVAL POSTGRADUATE SCHOOL
December 1973

ABSTRACT

An acoustic energy reflection experiment was conducted in a laboratory tank containing water and an artificial kaolin sediment. The reflection coefficient for the sediment was measured for a limited range of angles of incidence at one frequency and one set of measured sediment mass physical and viscoelastic properties. A mathematical reflection model was derived in terms of the known sediment properties. The measured and the theoretically calculated reflection coefficients are compared. The measured reflection coefficient and a probable angle of intromission showed poor agreement with theoretically predicted values. For the sediment parameters of the relatively soft clay used here, the reflection model is quite sensitive to values of sediment density and sound speed and is only mildly sensitive to values of dynamic rigidity and sound absorption coefficient near the angle of intromission.

TABLE OF CONTENTS

LIST OF TABLES

LIST OF FIGURES

ACKNOWLEDGMENT

The author wishes to express his gratitude to Professor O. B. Wilson, Jr. and to Professor R. S. Andrews for their patience, encouragement and advice throughout the course of this research. Thanks and appreciation are also extended to Mr. Robert Moeller for the construction of the mechanical devices used during the project. The project received partial support through contract with the Office of Naval Research, Ocean Sciences and Technology Division.

I. INTRODUCTION

A. BACKGROUND

The development and use of bottom bounce sonar and long range passive detection systems, and the use of sonar in shallow water all require knowledge of the effect the ocean bottom has on sound propagation loss. This effect is most often characterized by the quantity bottom loss (BL) in decibels, which is related to the reflection coefficient (R), the ratio of the reflected acoustic intensity to the incident acoustic intensity, by the equation $BL = -10 \log_{10} R$. The large variations in bottom loss throughout the world ocean bottoms, coupled with the passive or active sonar figure of merit sensitivity to small changes in this parameter, dictate a need for accurate measurement of bottom loss characteristics in each area of the oceans where bottom sediment parameters are different.

A direct method for collecting such information would be an oceanographic survey, of massive proportions, to determine the acoustic reflection coefficient at various angles of incidence and various frequencies of interest in each distinct bottom region of the world's oceans. On the other hand, surveys of other physical characteristics of the ocean bottoms have been going on for years, with the result that some core samples and raw and analyzed data exist for practically every oceanic bottom region. Although much information is available in the literature concerning the relation of reflection and transmission of acoustic energy to the properties of the reflecting and transmitting

media, a round table of exploration geophysicists concluded recently that their understanding of the "nature of seismic reflection is far from complete."* In anti-submarine and submarine warfare, where the exact nature of the reflection and transmission of acoustic energy at the ocean bottom must be well known, models for calculation of reflection coefficients generally are limited to consideration of a plane, homogeneous, compressional wave, transmitted at various angles of incidence in water and reflected from and refracted in layered sediments having various densities and other physical properties, including acoustic energy attenuation.

The energy loss a plane compressional wave undergoes upon reflection from the ocean's bottom is examined in a number of reports, papers and textbooks. Three of these references were chosen to describe the nature of the problem examined in this paper. White [1] was used as a basic text which describes the energy loss as a result of both compressional and shear waves being refracted in the sediment. Hamilton [2] uses the physical properties of density, compressional and shear wave speeds, along with related values of bulk modulus (K) and modulus of dynamic rigidity (μ) in the sediment to predict values of reflection coefficient and bottom loss. Hamilton treats the sediment as both an elastic and a viscoelastic medium. Bucker et al[3]compares measured and theoretically calculated values of bottom loss for multi-layered viscoelastic ocean sediments.

---

*Anstey, N. A., and Allen, S. J., "What Direction Should We Set for Hydrocarbon Exploration?" Exploration Geophysics, Vol. 21, No. 3, p. 412-421, September 1973

A number of the acoustic reflection experiments that have been conducted at sea, such as those referenced in [2] and [3], have shown varying degrees of agreement between theory and experiment. The disagreement usually is greatest near the critical angle or angle of intromission. The theoretical modeling of these experiments has been complicated by sediment layering and other non-uniformities and by difficulty in obtaining realistic physical properties. A laboratory experiment involving a smooth-surfaced homogeneous sediment and an undisturbed water layer helps to eliminate some of these complications in comparing measured and theoretical reflection coefficients.

B. DYNAMIC RIGIDITY

A key element in improved acoustic reflection models has been the inclusion of the dynamic rigidity and dissipation properties of the sediment. Most researchers, such as Hamilton [2] and Bucker et al [3], used measured Stoneley wave speeds to calculate the real part of dynamic rigidity. Only estimates of the imaginary part were available. Also, Stoke's assumption that in a viscoelastic fluid the bulk viscosity is equal to zero was employed by these researchers to estimate a value of the imaginary part of the first Lamé constant (λ).

At the Naval Postgraduate School, the torsional oscillator method has been used to measure the real and imaginary parts of the complex dynamic rigidity. Cohen [4] described one set of these measurements for a saturated, water-kaolin artificial sediment, and Martinek [5], conducting research on the same type of sediment, measured values of absorption coefficient.

C. REFLECTION COEFFICIENT

An objective of this research was to examine the usefulness and validity of the values of dynamic rigidity and absorption coefficient, along with other data on the physical properties of the sediment, in calculations with a viscoelastic reflection model, and to compare the calculated results with experimental reflection coefficients. The viscoelastic reflection model of Bucker et al [3] was modified to avoid the use of the assumption that the bulk viscosity is zero for a compressional wave. Some preliminary experimental measurements were made of the reflection coefficient at one frequency and for one sediment condition for comparison purposes.

II. THEORETICAL REFLECTION COEFFICIENT

A. DESCRIPTION OF THE MATHEMATICAL MODEL

Figure 1 illustrates a plane wave reflection model which was assumed to be an approximation to the experiment. The symbols and notation defined in Figure 1 were drawn from Bucker et al [3]. Referring to this figure, ϕ and Ψ are potential functions defined in the following paragraph and x is positive to the right while z is positive downward.

A summary of the development of water-sediment interface equations in [3] follows. The wave equation is given by the relationship $\nabla^2\phi + (\frac{\omega}{\alpha})^2 \phi = 0$, and its assumed potential function solutions are: (1)

$$\phi'_2 = A'_2 \exp i(kx + a_2kz - \omega t), \tag{2}$$

$$\phi'_1 = A'_1 \exp i(kx + a_1kz - \omega t), \tag{3}$$

$$\phi''_2 = A''_2 \exp i(kx - a_2kz - \omega t), \tag{4}$$

$$\Psi'_1 = B'_1 \exp i(kx + b_1kz - \omega t), \tag{5}$$

$$A''_1 = 0 , \quad B''_1 = 0 .$$

In water only the real values of k are considered for

$$k = \frac{\omega \sin \theta_i}{c_w} . \tag{6}$$

The term c_w is the measured speed of a compressional wave in water, A'_2 and A''_2 are the measured amplitudes of the incident and reflected waves, respectively, A'_1 and B'_1 are unknown quantities, θ_i is the angle of incidence, and ϕ''_1 and Ψ''_1 are both equal zero.

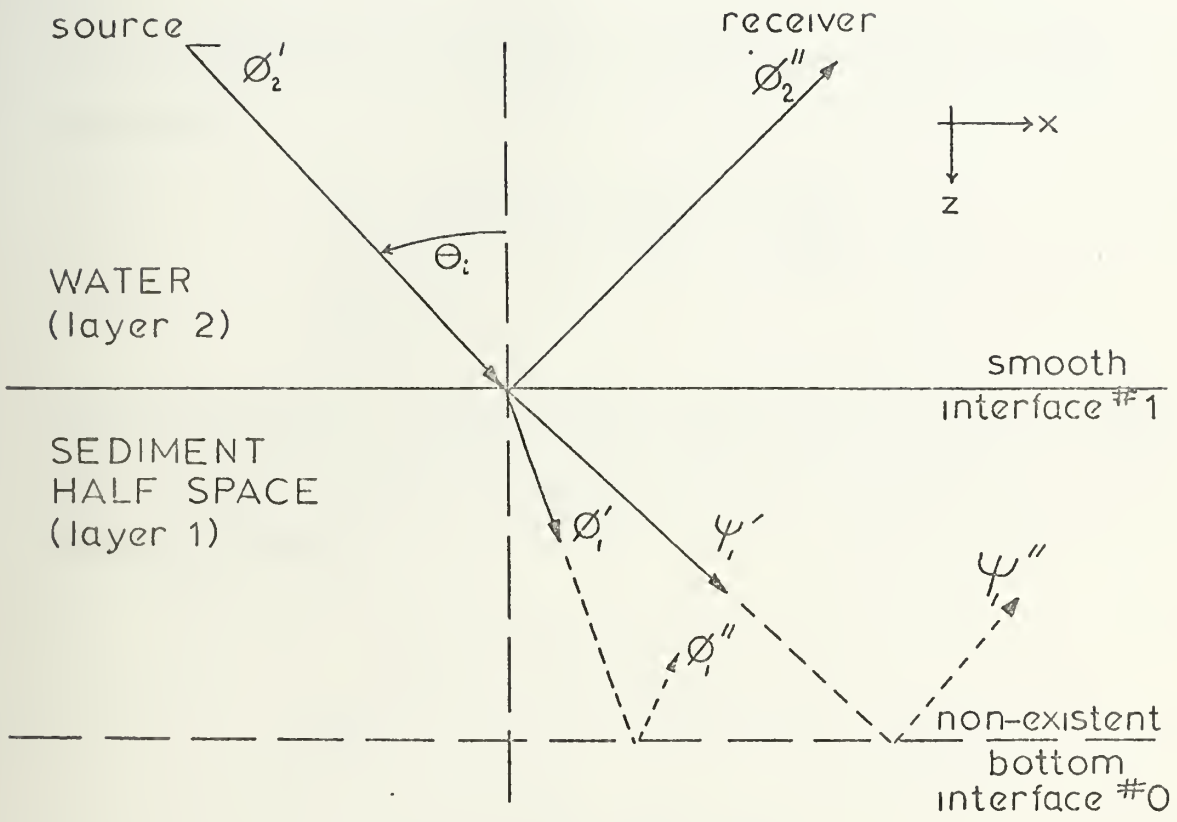

Figure 1. Theoretical Reflection Model.

For the water-sediment interface two boundary conditions may be applied to the potential function:

1. the vertical particle velocities (w) are continuous across the interface;

$$w = \frac{\partial \phi}{\partial z} + \frac{\partial \Psi}{\partial x} \tag{7}$$

2. the vertical stress-tensor elements are continuous across the interface;

$$p_{zz} = \frac{i}{\omega}(-\rho\omega^2\phi - 2\mu \frac{\partial^2\phi}{\partial x^2} + 2\mu \frac{\partial^2\Psi}{\partial x \partial z}) \tag{8}$$

$$p_{zx} = 0 .$$

Following Bucker [3], three interface equations are derived as follows from the boundary conditions and treatment of the sediment as a visco-elastic half-space;

$$a_2(A'_2 - A''_2) = a_1 A'_1 + B'_1 \tag{9}$$

$$\rho_2 (\frac{\omega}{k})^2 (A'_2 + A''_2) = \mu_1[(b_1^2-1)(A'_1) + 2b_1(B'_1)] \tag{10}$$

$$2a_1 (A'_1) = (b_1^2-1) B'_1 \tag{11}$$

where:

$$a_1^2 = \frac{\rho_1 c^2}{\lambda_1 + 2\mu_1} - 1 \tag{12}$$

$$b_1^2 = \frac{\rho_1 c^2}{\mu_1} - 1 \tag{13}$$

$$c = \frac{c_w}{\sin \theta_i} = \text{horizontal phase speed in water}$$

$$a_2 = \cot \theta_i$$

ρ_1 = density of sediment

ρ_2 = density of water

The Lamé constants λ and μ are complex,

$$\lambda_1 = \lambda'_1 - i\lambda''_1 \tag{14}$$

$$\mu_1 = \mu'_1 - i\mu''_1 \, . \tag{15}$$

B. SEDIMENT PARAMETERS

The above model permits a solution to the wave equation in terms of sediment parameters λ, μ, ρ and c, of which λ is the only term which does not have independently determined values. Cohen [4] measured values of dynamic rigidity, μ'_1 and μ''_1 for a range of sediment densities. Martinek [5] measured the absorption coefficient, a_p, and the compressional wave speed in the sediment, c_1, at a sediment density comparable to Cohen's and at frequencies in the range of experimental interest. These values are summarized in Table I of Section IV. Additional sound speed and density values were measured as part of this experiment and recorded in Table II of Section IV.

In the absence of scattering from the water-sediment interface, a_p in theory is related to λ''_1 and μ''_1 and c_1 is related to λ'_1 and μ'_1. With these known quantities, the next series of steps transposes the equations to eliminate λ'_1 and λ''_1 as independent variables and solves for a reflection coefficient in terms of sediment parameters μ'_1, μ''_1, ρ_1, c_1, along with c_w, ρ_2 and θ_i in the water layer.

C. CALCULATION OF REFLECTION COEFFICIENT

In the following development, the symbols are similar to those used by Borcherdt [6] but with a reversed sign convention for the complex exponential. The sign convention used here is the same used by Bucker et al [3]. Definition of terms is as follows:

$$k = k' - ik'' = \frac{\omega}{\alpha} = \text{complex propagation constant}$$

$$\alpha = \alpha' - i\alpha'' = \text{complex wave speed and}$$

$$\omega = \text{angular frequency}$$

$$\alpha = \text{p.v.} \left[\frac{K_1 + \frac{4}{3}\mu_1}{\rho_1} \right]^{1/2}$$

where K_1 is the bulk modulus and p.v. indicates principal value.

From Hamilton [2], $K_1 + \frac{4}{3}\mu_1 = \lambda_1 + 2\mu_1$ so that

$$\alpha = \text{p.v.} \left(\frac{\lambda_1 + 2\mu_1}{\rho_1} \right)^{1/2} . \tag{16}$$

The compressional wave speed in the sediment, c_1, is given by

$$\frac{1}{c_1} = \text{Re} \left[\frac{1}{\alpha} \right] . \tag{17}$$

The compressional wave absorption coefficient in the sediment is

$$a_p = \omega \text{Im} \left[\frac{1}{\alpha} \right] . \tag{18}$$

The complex compressional wave propagation constant is

$$k = \frac{\omega\alpha'}{|\alpha|^2} + i \frac{\omega\alpha''}{|\alpha|^2} = \frac{\omega}{c_1} + ia_p .$$

For physical reasons, $a_p \geq 0$ to ensure decreasing values of the potential function with positive increasing values of distance along the propagation path. By the same physical reasoning, $c_1 \geq 0$.

Algebraic steps to solve for reflection coefficient, R, in terms of μ'_1, μ''_1, c_1, a_p and frequency, f, and independent of λ'_1 and λ''_1 are shown in detail in Appendix A. These steps yield the following set of equations:

$$R \equiv \left| \frac{A''_2}{A'_1} \right|^2 = \left| \frac{Z-1}{Z+1} \right|^2 \qquad \text{(A-10)(A-11)}$$

$$Z = \frac{A'_2 + A''_2}{A'_2 - A''_2} = \left(\frac{2a_2 \mu_1 k^2}{\rho_2 (b_1^2+1)\omega^2} \right) \left(\frac{(b_1^2-1)^2}{2a_1} + 2b_1 \right) \qquad \text{(A-9)}$$

$$a_1^2 = H + iJ \qquad \text{(A-12)}$$

$$b_1^2 = F + iG \qquad \text{(A-15)}$$

$$F = \frac{\rho_1 c^2 \mu'_1}{(\mu'_1)^2 + (\mu''_1)^2} - 1 \qquad \text{(A-16)}$$

$$G = \frac{\rho_1 c^2 \mu''_1}{(\mu'_1)^2 + (\mu''_1)^2} \qquad \text{(A-17)}$$

$$H = \rho_1 c^2 \left(\frac{1}{c_1^2} - \frac{1}{4} \left(\frac{a_p}{\pi f} \right)^2 \right) - 1 \qquad \text{(A-18)}$$

$$J = \left[\frac{\left(\frac{c_1 a_p}{\pi f} \right)}{1 - \left(\frac{c_1 a_p}{2\pi f} \right)^2} \right] \left(H + 1 \right) \qquad \text{(A-19)}$$

Equation (A-11) for R then was solved using standard WATFORG on the IBM 360 computer at the Naval Postgraduate School. Values of θ_i were chosen from zero to $\pi/2$ and the physical properties of the sediment were taken from Cohen [4] and Martinek [5]. Values for BL and R were computed over the range of experimental error measured in the physical properties cited in these two references, in order to examine them for sensitivity to changes in these values.

III. MEASUREMENT OF REFLECTION COEFFICIENT

A. SUMMARY OF THE EXPERIMENT

The experiment was conducted by reflecting a pulsed beam of sound from a water-sediment interface at various angles of incidence. The incident and reflected wave amplitudes were detected with a directional receiver of design identical to that of the transmitter. A sound frequency of 120 kHz was used. The received signals were amplified, filtered and signal processed to improve signal-to-noise ratio. The reflection coefficient was computed from the ratio of the squares of the voltage amplitude of the direct and sediment reflected pulses, using appropriate corrections for spherical divergence.

B. THE APPARATUS

The artificial sediment, a commercially available pure kaolinite, was contained in a large, rectangular tank, 2.42 m long by 1.20 m wide by 1.00 m deep. The leveled, saturated sediment thickness was 60 cm. The water depth was 31.5 cm.

Identical transmitting and receiving transducers were set up in the water and mounted on a horizontal rail above the tank. Each transducer could be rotated through 360° independently in both the vertical and horizontal axes and moved horizontally and vertically in the tank. The two electrostatic type transducers, built by research physicist Donald F. Spiel of the Naval Postgraduate School, have an active circular face of 6.0 cm diameter, consisting of an aluminum coated, one mil thick plastic film mounted over an aluminum electrode which is set in

a larger plastic disc. In order to keep the air gap between the plastic film and the electrode uniform, equalization of pressure between this gap and an air filled space behind the electrode was achieved by small holes drilled in the aluminum electrode. The inside of the transducer was partially evacuated. At 120 kHz the 3 dB beam width is about 20°.

The basic geometry of the experiment is shown in Figure 2. Referring to this figure, both the transmitting and receiving transducers were rotated to a selected angle of incidence, θ_i.

Based on the choice of centerline height of each transducer being 23.5 cm above the sediment layer, the idealized ray path y_1 was computed for each θ_1 and the transducers were positioned along the horizontal rail so that $y_1 = y_2$ and $x_1 = x_2$. The horizontal placement also was chosen to ensure that the same region of sediment was ensonified for each case.

The range of angles accessible for this experiment is limited by the dimensions of the apparatus and the necessity to keep the sediment reflecting surface in the far field region of the directional transducers. The extent of the far field region was determined experimentally by plotting the directly propagated sound field pressure as a function of range.

The directivity of both transducers at 120 kHz provided a sufficient reduction in off-axis signals to eliminate interference from side wall and water-air surface reflections. This was confirmed experimentally. At angles above 70° a small amount of interference between direct and sediment reflected pulses could be observed, the effects of which are discussed later.

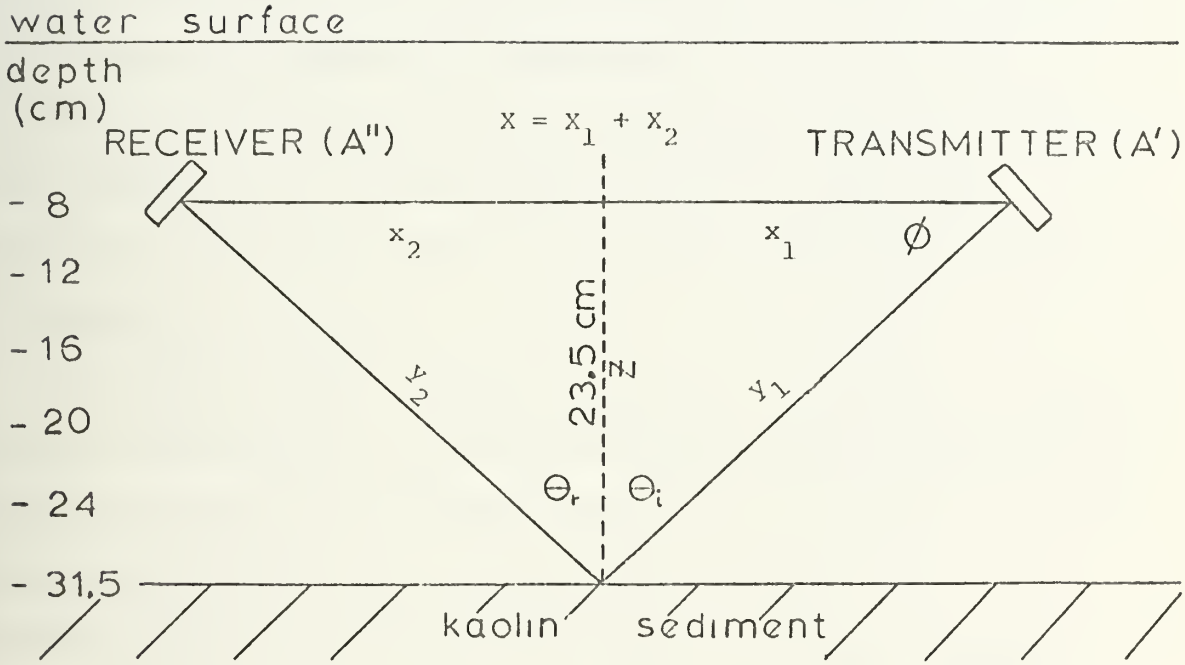

Figure 2. Experiment Geometry.

C. INSTRUMENTATION

Figure 3 illustrates the transmitting and receiving equipment and circuitry in block diagram form. This configuration is similar to that used by Martinek [5]. The Hewlett Packard 204C oscillator frequency was set at 120 kHz within $\pm$ 3 Hz and was monitored with a frequency counter. The General Radio 1396-A tone burst generator was set to produce two-cycle tone burst pulses with an approximate 10 msec delay between pulses. This delay was sufficient to prevent undesired reflections from disturbing the measurements. The Hewlett Packard 467A amplifier was used to boost the voltage by a factor of ten before the signal went to a 1:3 transformer for further amplification. The polarizing circuits for both the electrostatic transducers are shown in Figure 4.

The received signal was amplified either 20 or 40 dB by a Hewlett Packard 465A amplifier and then passed through Krohn-Hite high and low pass filters set to a 20 kHz pass band centered at 120 kHz. A Princeton Applied Research (PAR) model 160 boxcar integrator was used for signal processing. The time delay feature of the boxcar integrator was used to determine the times of pulse arrival. The enhanced signal from the arriving pulse was then fed to a Moseley X-Y Recorder. Figure 5 which was traced from original records represents typical received wave forms after integration and recording. Wave form points selected to determine zero to peak voltages are noted on this figure.

D. DATA COLLECTION PROCESS AND ERROR ANALYSIS

A number of angles of incidence were selected and appropriate horizontal separations were pre-calculated. At each setting of horizontal

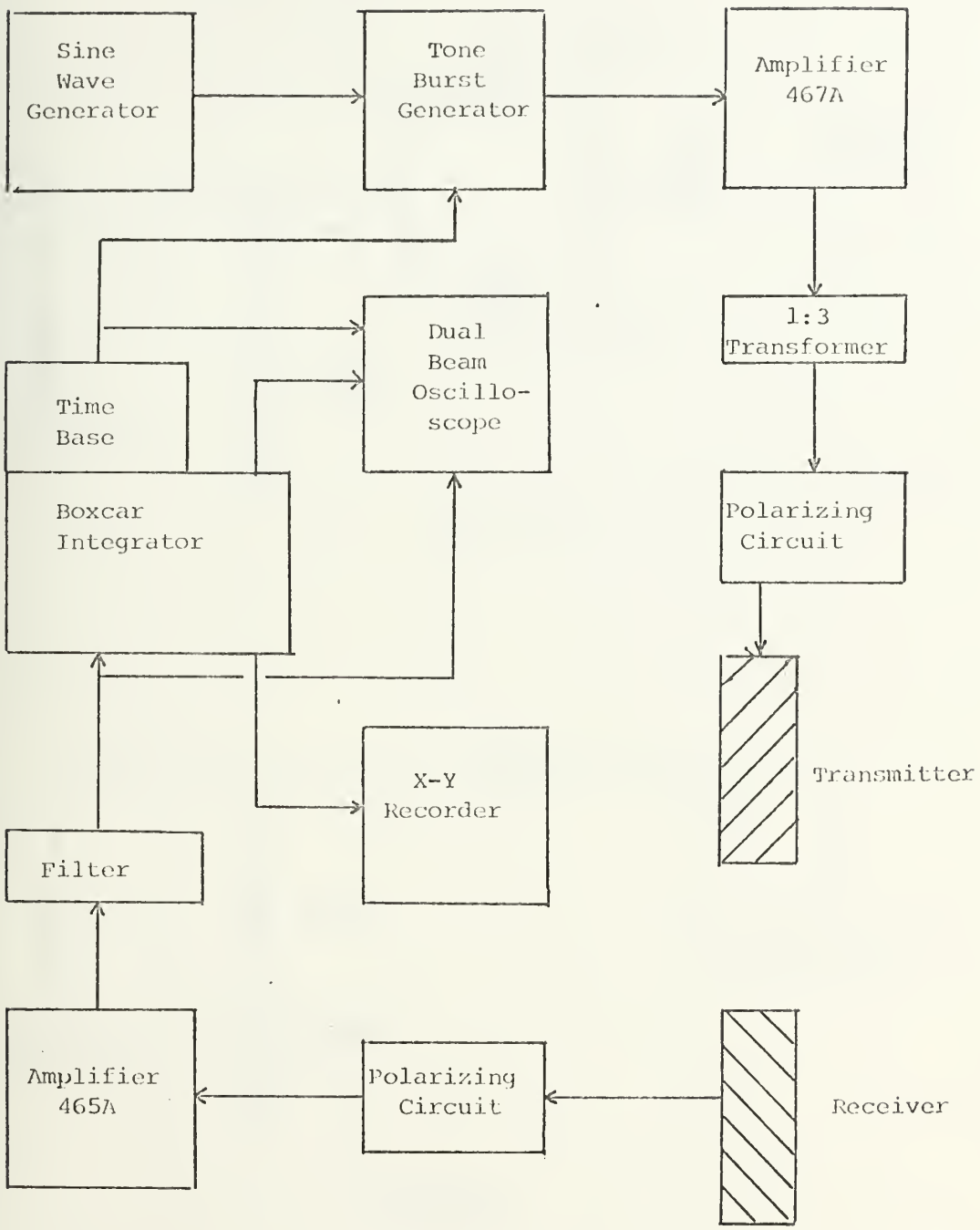

Figure 3. Instrumentation.

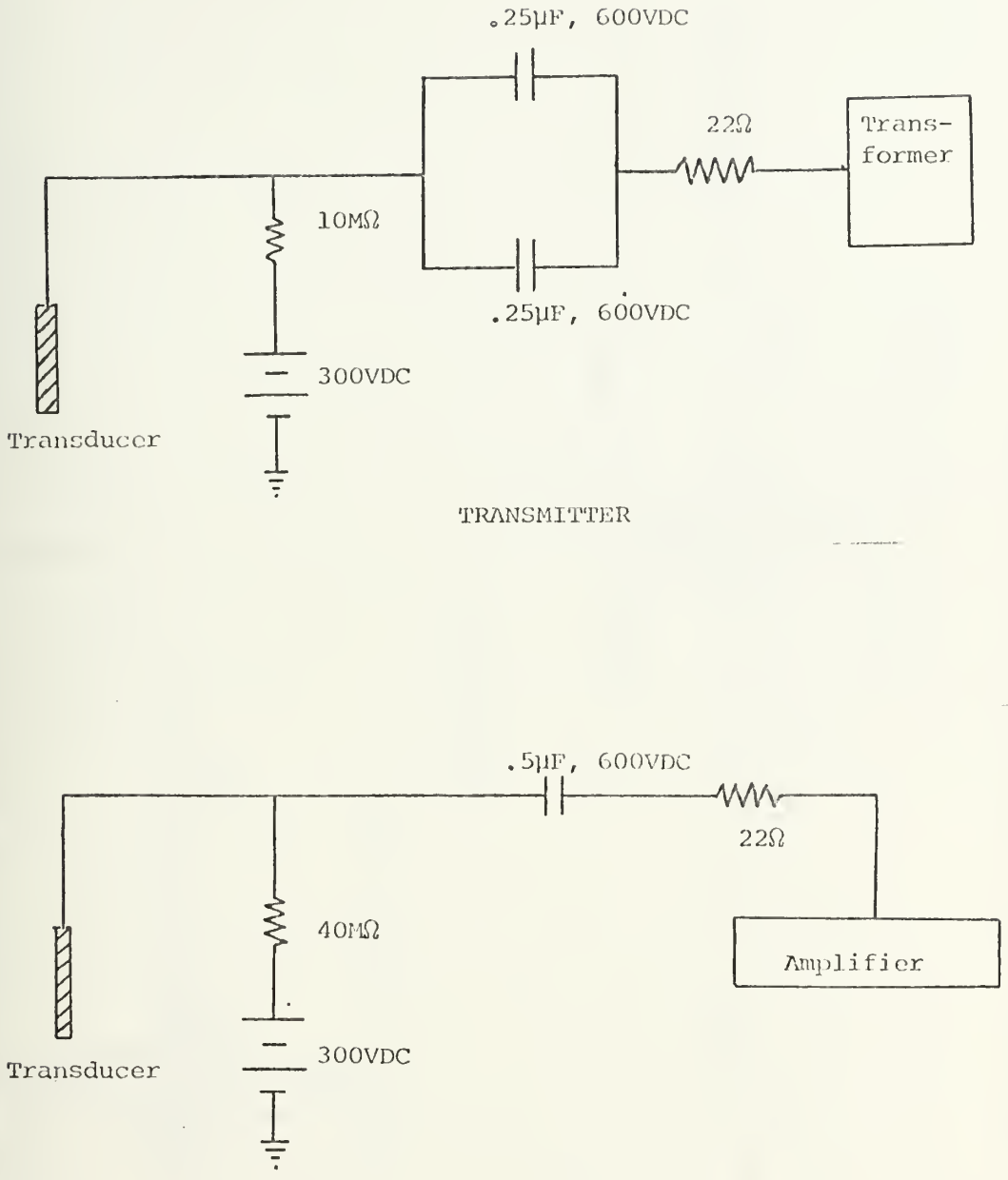

Figure 4. Polarizing Circuits.

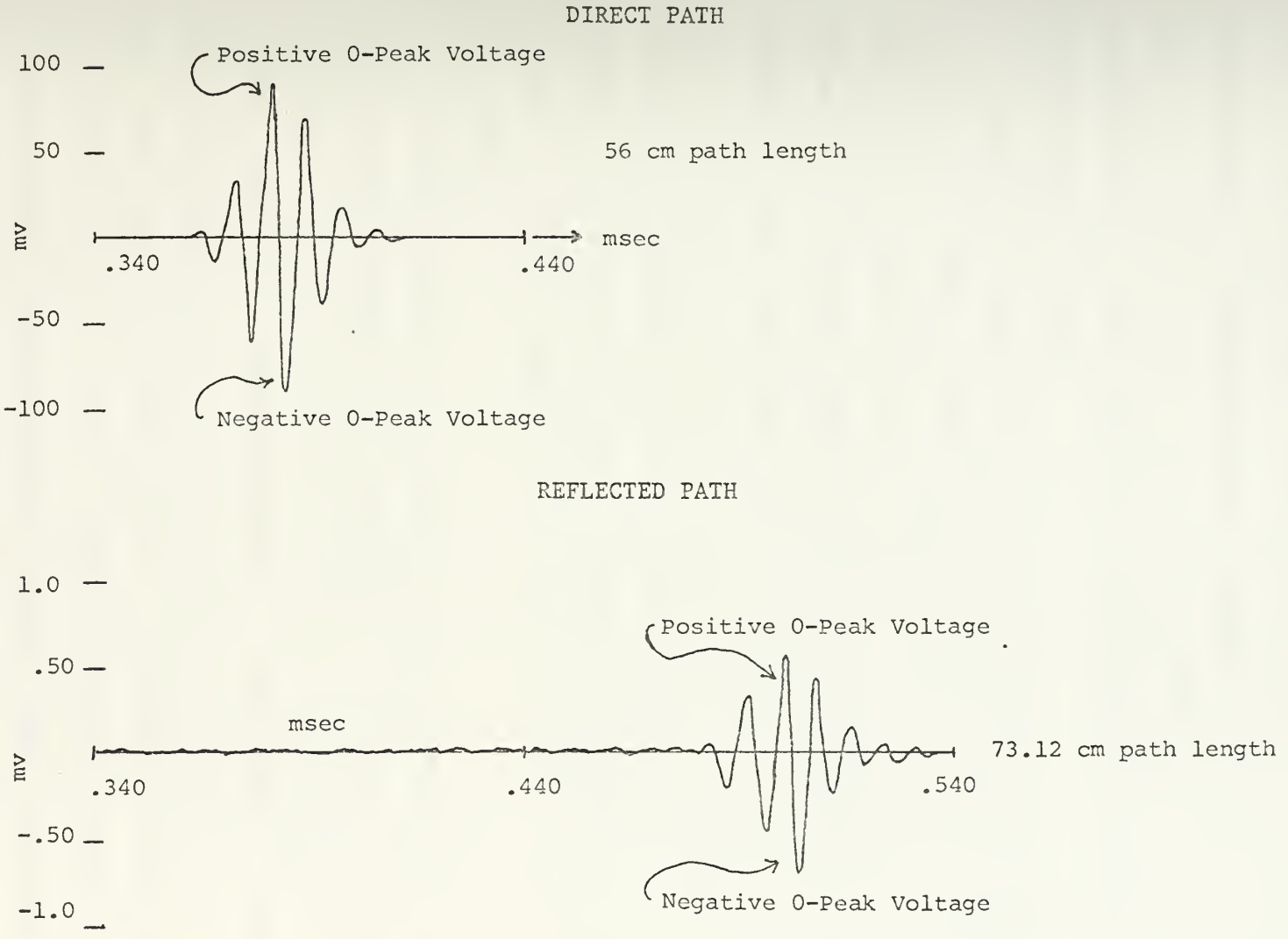

Figure 5. Comparison of Direct Path and Reflected Wave Forms.

spacing, measurements were recorded of the received pulses for both a direct path between source and receiver ($\theta_i = 0$) and for the sediment reflected path. Additional gain was required for the latter measurement. The receiver then was moved its full horizontal travel to determine that no other pulses were being reflected from below the water-sediment interface.

Referring to Figure 5, zero to peak voltage was determined by averaging the maximum positive and negative peaks of each recorded pulse. In all cases these peaks occurred in the third cycle of the pulse. Voltage output anomalies in the tone burst generator, transformers, filters, amplifiers, boxcar integrator and the X-Y recorder were assumed to be the same for both direct path and reflected path voltages and therefore were cancelled by division in the reflection coefficient ratio. Also, because of this ratio computation, transducer sensitivities, sound pressure level calculations, etc., were not required.

The log-log plot of direct path average zero to peak amplitude versus horizontal separation was constructed to determine the minimum horizontal separation at which the pressure varies linearly with the inverse range (1/r). This established the inner limits of horizontal separation which in turn set the minimum angle of incidence at $\theta_i = 50°$. Since the reflected path was longer than the direct path, this separation insured that the ensonified patch of sediment was also in the far field. The dimensions of the tank limited the maximum angle of incidence to $\theta_i = 76°$.

The arrival time of the sediment reflected pulse occurred later than the arrival time of the direct pulse. The measured arrival time

differences between the two pulses were compared with time differences calculated using the idealized geometry ray path difference and the known speed of sound. Compatibility between observed and calculated delays confirmed detection of the sediment reflected signal.

The uncertainty in the angle of incidence (θ_i) on each transducer is about $\pm$ 1.0°. Part of this is due to the precision with which the scale could be read and part arises in the assembly process of aligning the transducer face to the zero mark on the angle indicator dial. It is estimated that horizontal separations were accurate to $\pm$ 0.2 cm. The height of the transducer above the ensonified sediment patch was accurate to $\pm$ 0.2 cm and the sediment surface within the ensonified patch was level and smooth within $\pm$ 0.1 cm. With a sound wavelength of about 1.2 cm, this scale of roughness in bottom level is considered not to have a significant effect on observed signal amplitudes. The uncertainty in measuring voltage amplitude is estimated to be 2% of the millivolt scale in Figure 5.

At angles of incidence greater than 70°, small but perceptible off-axis energy from the direct path was detected. Since the difference between reflected and direct path lengths decreases with greater angle of incidence, the arrival time difference between the two pulses decreased so that the leading edge of the reflected pulse overlapped the tail of the direct path off-axis pulse. This resulted in an estimated $\pm$ 5% error in reflected voltage amplitudes above 70°.

E. THEORY OF MEASUREMENT

Referring to Figure 2, it was assumed that the sound pressure amplitude varied inversely as the square of the range from the source and

that the absorption in the water was negligible. The assumption was also made that the sediment surface was sufficiently smooth and homogeneous so that the reflected rays behaved as if they had originated at the mirror image position of the source.

The received intensity I, at any range x along the direct path, was determined by orienting the beam axes of the transducers toward each other and measuring signal amplitude A'. Intensity I is proportional to $(A')^2$. The reflected wave intensity I_r, which is proportional to the square of the measured reflected wave amplitude A', is a function of the reflection coefficient R, I_1, and the spherical spreading along the total reflected path length $y = y_1 + y_2 = 2y_1$, assuming that the reflection is specular. I_1 is the axial intensity at unit distance from the sound projector. Stated in equation form, this relation is $I_r = (A")^2 = RI_1/y^2$. Solving for R and substituting for I_1 determined from the direct path measurements gives the following:

$$R = \left(\frac{2A"y_1}{A'x} \right)^2$$

Bottom loss is calculated by

$$BL = -10 \log_{10} R \text{ (dB)}.$$

IV. PRESENTATION OF DATA

Tables I and II, which list some of the mass physical properties of the sediment, are self-explanatory. Table II records the speed of sound and density in the sediment for three different depths near the surface. Sound speed ratio c_1/c_w was measured with a sound velocimeter and densities were measured using the sampling device described by Martinek [5]. The data show both density and velocity gradients in the upper part of the sediment.

Table III lists a series of eight combinations of the five measured sediment parameters which are used in the theoretical model. These combinations are designed to determine the model's sensitivity to parameter changes with each combination given a sequence number for reference purposes. Sequence (1) is based on Table I dynamic rigidities at a density of 1.35 gm/cm^3 along with sound speed and absorption coefficient at a density of 1.38 gm/cm^3. The maximum positive experimental error from Table I dynamic rigidities is the change inserted in Sequence (2). The effect of only a density change from 1.38 gm/cm^3 to 1.28 gm/cm^3 is determined from using Sequence (3). Together, Sequence (2) and (3) test the model for sensitivity to density changes. Sequence (4) shifts to the Table I values of dynamic rigidity for 1.28 gm/cm^3 density and in Sequence (5) the measured sound speed for a density of 1.28 gm/cm^3 in Table III is inserted. Together, Sequence (4) and (5) determine the effect of only a sediment sound speed change. Also, Sequence (5) is based on the measured data which is assumed to be the closest approximation to the sediment conditions during the reflection experiment.

Sequence (6) and (7) are designed to test the model for large arbitrary changes in dynamic rigidity. The density of 1.24 gm/cm^3 is an assumed value of sediment density at a point closer to the surface than that at which a suitable sample could be collected. Sequence (8) tests the model for a large arbitrary change in absorption coefficient relative to that in Sequence (5).

Tables IVa and IVb tabulate the values of R and BL for the eight sequences computed from Equation (A-11) for a range of angles of incidence from 14° to 83°. From these two tables sensitivity of the theoretical model is determined. The values from Sequences (1) and (5) are plotted in Figure 6 for comparison.

Table V tabulates the data from the reflection experiment. The values of BL in this table are plotted in Figure 6 along with calculated values from Sequences (1) and (5).

TABLE I

Physical Properties of Saturated Water-Kaolin Sediment

Cohen [4] Sediment Properties for 20°C

Density	Dynamic Rigidity	
ρ_1 (gm/cm^3)	μ'_1 x 10^{-4} (dynes/cm^2)	μ''_1 x 10^{-4} (dynes/cm^2)
1.28	26.6 $\pm$ 3.4	2.85 $\pm$ 1.20
1.31	54.8 $\pm$ 7.4	9.68 $\pm$ 4.36
1.35	67.9 $\pm$14.5	16.6 $\pm$ 6.90

Martinek [5] Sediment Properties for 19.9°C

Frequency	Density	Sound Speed **	Absorption Coefficient
f (kHz)	ρ_1 (gm/cm^3)	c_1 (cm/sec)	a_p (nepers/cm)
100	1.38	1422 x 10^2	3.79 x 10^{-3}
125	1.38	1422 x 10^2	4.83 x 10^{-3}
* 120	1.38	1422 x 10^2	4.62 x 10^{-3}

* Linear interpolation from 100 and 125 kHz data

** $c_1/c_w = 0.94$

TABLE II

Measured Sound Speed and Densities

Average Sediment Depth (cm)	Average Sediment Density (gm/cm^3)	$\frac{c_1}{c_w}$ at Depth* (cm)	c_1** (cm/sec)
1.55 (Surface sample)	1.28 ± .05	0.974 at 1.37	1442×10^2
3.85	1.38 ± .05	0.965 at 3.39	1428×10^2
7.85	1.42 ± .05	Not measured	-

*Measured at 18.8°C

**Corrected to 20°C, based on $c_w = 1480 \times 10^2$ cm/sec

TABLE III

Combinations of Sediment Parameters
Used in Theoretical Computations

Sequence No.	μ'_1 (dynes/cm^2)	μ''_1 (dynes/cm^2)	ρ_1 (gm/cm^3)	c_1 (cm/sec)	a_p (nepers/cm)
1.	67.9×10^4	16.6×10^4	1.38	1.422×10^5	0.462×10^{-4}
2.	82.4×10^4	23.5×10^4	1.38	1.422×10^5	0.462×10^{-4}
3.	82.4×10^4	23.5×10^4	1.28	1.422×10^5	0.462×10^{-4}
4.	26.6×10^4	2.85×10^4	1.28	1.422×10^5	0.462×10^{-4}
5.	26.6×10^4	2.85×10^4	1.28	1.442×10^5	0.462×10^{-4}
6.	266	28.5	1.24	1.450×10^5	0.462×10^{-4}
7.	26.6×10^8	2.85×10^8	1.24	1.450×10^5	0.462×10^{-4}
8.	26.6×10^4	2.85×10^4	1.28	1.442×10^5	0.462×10^{-2}

TABLE IVa

Calculation of Reflection Coefficient and Bottom Loss
Sequences 1-4

Angle of Incidence θ_i	Sequence No. (From Table III)							
	1		2		3		4	
	$R \times 10^2$	BL(dB)	$R \times 10^2$	B_L(dB)	$R \times 10^2$	B_L(dB)	$R \times 10^2$	BL(dB)
14.3°	0.315	25.0	0.315	25.0	0.145	28.4	0.146	28.4
20.1	0.257	25.9	0.257	25.9	0.113	29.5	0.113	29.5
28.7	0.144	28.4	0.144	28.4	0.0517	32.9	0.0517	32.9
34.4	0.0650	31.9	0.0650	31.9	0.0145	38.4	0.0145	38.4
37.2	0.0315	35.0	0.0315	35.0	0.00287	45.4	0.00289	45.4
40.1	0.00770	41.1	0.00770	41.0	0.583×10^{-3}	52.3	0.576×10^{-3}	52.4
42.9	0.264×10^{-3}	55.8	0.266×10^{-3}	55.8	0.0131	38.8	0.0131	38.8
45.8	0.0188	37.3	0.0188	37.3	0.0485	33.1	0.0485	33.1
48.6	0.0769	31.1	0.0769	31.1	0.118	29.3	0.118	29.3
54.4	0.399	24.0	0.399	24.0	0.436	23.6	0.436	23.6
63.0	2.05	16.9	2.05	16.9	1.93	17.1	1.93	17.1
71.6	7.70	11.3	7.70	11.3	7.06	11.5	7.06	11.5
83.0	38.6	4.13	38.6	41.3	36.9	4.32	36.9	4.32

TABLE IVb

Calculation of Reflection Coefficient and Bottom Loss
Sequences 5-8

Angle of Incidence θ_i	Sequence No. (From Table III)							
	5		6		7		8	
	R x 10^2	BL(dB)	R x 10^2	BL(dB)	R x 10^2	BL(dB)	R x 10^2	BL(dB)
14.3°	0.207	26.8	0.167	27.8	0.158	28.0	0.207	26.8
20.1	0.170	27.7	0.138	28.6	0.123	29.1	0.170	27.7
28.7	0.0969	30.1	0.0796	31.0	0.0584	32.3	0.0969	30.1
34.4	0.0448	33.5	0.0377	34.2	0.0189	37.2	0.0448	33.5
37.2	0.0222	36.5	0.0192	37.2	0.00541	42.7	0.0222	36.5
40.1	0.00582	42.4	0.00544	42.6	0.447×10^{-4}	63.5	0.00586	42.3
42.9	0.763×10^{-4}	61.2	0.480×10^{-5}	73.2	0.00737	41.3	0.122×10^{-3}	59.1
45.8	0.0117	39.3	0.00835	40.8	0.0339	34.7	0.0117	39.3
48.6	0.0506	33.0	0.0386	34.1	0.0890	30.5	0.0506	33.0
54.4	0.275	25.6	0.220	26.6	0.347	24.6	0.275	25.6
63.0	1.50	18.2	1.25	19.0	1.59	18.0	1.50	18.2
71.6	6.08	12.2	5.28	12.8	6.03	12.2	6.08	12.2
83.0	35.0	4.56	33.0	4.82	34.4	4.63	35.0	4.56

TABLE V

Measured Reflection Coefficient and Bottom Loss

Angle of Incidence θ_i (degrees)	Horizontal Separation x (cm)	Reflected Path Length y_1+y_2 (cm)	Path Length Difference (cm)	Direct Path 0-Peak Avg. volts (mv)	Reflected Path 0-Peak Avg. volts (mv)	Reflection Coefficient $R \times 10^4$	Bottom Loss BL (dB)
50	56.02	73.12	17.10	96.5	0.625	0.715	41.5
55	67.12	81.94	14.82	84.0	0.550	0.639	42.0
60	81.40	94.00	12.60	71.5	0.440	0.505	42.9
65	100.80	111.62	10.82	58.5	0.375	0.500	43.0
70	129.14	137.42	8.28	45.0	0.335	0.628	42.0
72	144.16	152.10	7.44	41.5	0.300	0.578	42.3
74	163.90	170.52	6.62	35.0	0.305	0.822	40.9
76	188.50	194.28	5.78	31.5	0.375	1.506	38.2

Figure 6. Comparison of Results.

V. COMPARISON OF DATA

A comparison of the bottom loss calculations from the reflection model with the measured results from the experiment reveals somewhat poor agreement between the two. The experimental limits on the angles of incidence prevented measuring reflection coefficients in the vicinity of the theoretically predicted values of 40° to 43°. Figure 6 shows a possible measured angle of intromission in the vicinity of 65°, but the lack of experimental results below 50° leaves open the possibility of even higher measured bottom losses at the lower angles. An additional comparison was made with a liquid-liquid model described in Kinsler and Frey [7, p. 145], using only the densities and sound speeds of Sequences (1) and (5), which predicted an angle of intromission in the range of 26° to 27°. The theoretical magnitudes of bottom loss near the angle of intromission are 10 to 20 dB higher than the values measured at about 65°.

The eight combinations of parameter changes reveal a number of facts regarding the theoretical model and its application to the experiment performed. A summary of comparisons among sequences is contained in Table VI on the following page. The high sensitivity to density and sound speed changes shown in this table agrees with what is expected from the basic liquid-liquid model [7]. The Table VI comparisons also reveal that dynamic rigidity and absorption coefficient affect bottom loss magnitude only near the angle of intromission. The range of parameter changes selected for the sensitivity tests had only a small effect on the range of theoretical angles of intromission, as shown in Table VI.

TABLE VI

Comparison of Sequences

Sequence Numbers	Parameter Change	Sensitivity of Equation (A-11)
1 and 2	Small change in dynamic rigidity	Sensitive only at the angle of intromission
2 and 3	Density	Very sensitive
4 and 5	Sound Speed	Very sensitive
6 and 7	Large change in dynamic rigidity	Sensitive only near the angle of intromission
5 and 8	Absorption Coefficient	Low sensitivity only at angle of intromission

VI. CONCLUSIONS AND RECOMMENDATIONS

The data collected for one sediment condition at one frequency for a limited range of angles of incidence must be considered as preliminary in nature. Three extensions of data collection using the developed experimental method are needed to complete the experiments. A variation in sediment conditions is needed to measure the effect on reflection coefficient from known changes in density, sound speed and dynamic rigidity. Apparatus now exists to measure all of these parameters. A variation in frequency also is needed to measure the effect of changes in absorption coefficient, which has been assumed to be the only frequency dependent sediment property. Measurements over a wider range of angles of incidence are needed in order to determine experimentally the existence of an angle of intromission. In order to increase the range of angles of incidence changes in the apparatus will be required. As an example, a deeper and larger tank will permit measurements at smaller angles of incidence.

The low sensitivity of R to values of dynamic rigidity could be due to the range of dynamic rigidities used for the material not being representative. Because of the fact that the reflection model is quite sensitive to sound speed and density, there exists the possibility that a part of the discrepancy between calculated and observed reflection coefficients is due to inadequate accuracy for measured sediment physical properties.

The sediment densities and velocities measured during this experiment and earlier by Martinek [5] confirm that gradients in properties

do exist in the upper portion of the sediment. Although the gradients may have a significant influence on the observed reflection, this was not accounted for in the theoretical model used here and time limitations did not permit the adaptation of another model. One such model which does include sound velocity gradients in the reflecting medium has been developed by Morris [8] based on the theory of layered media reflections described by Brekhovskikh [9]. .The gradient models must be included for experiments in which the sound reflection process involves greater penetration of sound into the sediment than was probably the case in the experiment reported here.

APPENDIX A

Algebraic steps to solve for reflection coefficient in Section II are set forth in this appendix.

$$(\alpha)^2 \equiv x-iy = (x^2 + y^2)^{1/2}\, e^{-i\theta} = re^{-i\theta} \qquad \text{(A-1)}$$

Note: θ not related to θ_i

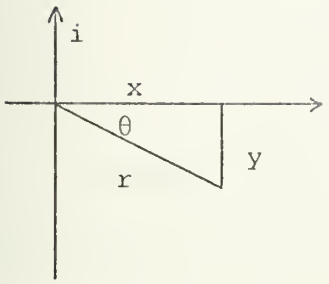

$$x \equiv \lambda'_1 + 2\mu'_1 \qquad \text{(A-2)}$$

$$y \equiv \lambda''_1 + 2\mu''_1 \qquad \text{(A-3)}$$

$$r \equiv (x^2 + y^2)^{1/2} \qquad \text{(A-4)}$$

$$\alpha = (r)^{1/2}\, e^{-i\,\theta/2} = (r)^{1/2}(\cos\,\theta/2 - i\,\sin\,\theta/2)$$

The positive roots of the following trigonometric identities were substituted:

$$\cos\,\theta/2 = \pm\,\left(\frac{1 + \cos\,\theta/2}{2}\right)^{1/2},\quad \sin\,\theta/2 = \pm\,\left(\frac{1 - \cos\,\theta/2}{2}\right)^{1/2}$$

$$\alpha = (r)^{1/2}\,\left\{\left[\left(\frac{1}{2}\right)\left(1+\frac{x}{r}\right)\right]^{1/2} - i\left[\left(\frac{1}{2}\right)\left(1-\frac{x}{r}\right)\right]^{1/2}\right\}$$

$$= \frac{1}{\sqrt{2}}\,\left[(r+x)^{1/2} - i(r-x)^{1/2}\right]$$

Rationalizing the inverse of the above to obtain $\frac{1}{\alpha}$ yields the following:

$$\frac{1}{\alpha} = \frac{(r+x)^{1/2} + i(r-x)^{1/2}}{r\sqrt{2}}$$

Substituting the real and imaginary parts into Equations (17) and (18) yields the following:

$$\mathrm{Re}\left[\frac{1}{\alpha}\right] = \frac{(r+x)^{1/2}}{r\sqrt{2}}$$

$$\mathrm{Im}\left[\frac{1}{\alpha}\right] = \frac{(r-x)^{1/2}}{r\sqrt{2}}$$

$$c_1 = \frac{r\sqrt{2}}{\sqrt{r+x}} \tag{A-5}$$

$$a_p = \frac{\sqrt{2}\,\pi f\sqrt{r-x}}{r} \tag{A-6}$$

Algebraic manipulation of c_1 and a_p then was used to eliminate r and state all relations in terms of x and y.

$$c_1^2 = \frac{2r^2}{r+x}\,, \qquad a_p = \frac{2(\pi f)^2(r-x)}{r^2}$$

$$r + x - \left(\frac{2}{c_1^2}\right) r^2 = 0$$

$$r - x - \frac{1}{2}\left(\frac{a_p}{\pi f}\right)^2 r^2 = 0$$

$$2x + r^2\left[\frac{1}{2}\left(\frac{a_p}{\pi f}\right)^2 - \frac{2}{c_1^2}\right] = 0$$

$$\frac{x}{r^2} = \left[\frac{1}{c_1^2} - \frac{1}{4}\left(\frac{a_p}{\pi f}\right)^2\right] \tag{A-7}$$

Manipulating further as follows:

$$(c_1)^2(a_p)^2 = \frac{(2\pi f)^2(r-x)}{r+x}$$

$$\left(\frac{c_1 a_p}{2\pi f}\right)^2 = \frac{r-x}{r+x}$$

$$\frac{x}{r} = \frac{1 - \left(\frac{c_1 a_p}{2\pi f}\right)^2}{1 + \left(\frac{c_1 a_p}{2\pi f}\right)^2} \quad .$$

From $r^2 = x^2 + y^2$, $\left(\frac{y}{r}\right)^2 = 1 - \left(\frac{x}{r}\right)^2$

$$\left(\frac{y}{r}\right)^2 = 1 - \left[\frac{1 - 2\left(\frac{c_1 a_p}{2\pi f}\right)^2 + \left(\frac{c_1 a_p}{2\pi f}\right)^4}{1 + 2\left(\frac{c_1 a_p}{2\pi f}\right)^2 + \left(\frac{c_1 a_p}{2\pi f}\right)^4}\right]$$

$$\left(\frac{y}{r}\right) = \pm \frac{\frac{c_1 a_p}{\pi f}}{1 + \left(\frac{c_1 a_p}{2\pi f}\right)^2}$$

and since a_p and c_1 are greater than zero, the positive root is chosen. Combining x/r and y/r to obtain y/x yields the following:

$$\frac{y}{x} = \frac{\frac{c_1 a_p}{\pi f}}{1 - \left(\frac{c_1 a_p}{2\pi f}\right)^2} \qquad \text{(A-8)}$$

Substituting the definitions of x, y and r^2 in Equations (A-2), (A-3) and (A-4) shows that μ'_1, μ''_1, λ'_1 and λ''_1 are related only to the groupings of known physical properties of Equations (A-7) and (A-8).

Solving the interface equations by adding Equation (9) and (11) and substituting the result into Equation (10) gives:

$$2a_2(A'_2 - A''_2) = B'_1(b_1^2 + 1)$$

$$\rho_2 \left(\frac{\omega}{k}\right)^2 (A'_2 + A''_2) = \mu_1 \left(\frac{(b_1^2 - 1)(b_1^2 - 1)B'_1}{2a_1} + 2b_1 B'_1 \right)$$

$$= \mu_1 B'_1 \left(\frac{(b_1^2 - 1)^2}{2a_1} + 2b_1 \right)$$

Substituting $$B'_1 = \frac{2a_2 (A'_2 - A''_2)}{(b_1^2 + 1)}$$

$$Z = \frac{A'_2 + A''_2}{A'_2 - A''_2} = \left[\frac{2a_2 \mu_1 k^2}{\rho_2 \omega^2 (b_1^2 + 1)} \right] \left[\frac{(b_1^2 - 1)^2}{2a_1} + 2b_1 \right] \qquad \text{(A-9)}$$

Letting Z equal the right hand side of Equation (A-9) and defining intensity reflection coefficient

$$R = \left| \frac{A''_2}{A'_2} \right|^2 \qquad \text{(A-10)}$$

such that $$\frac{A'_2 + A''_2}{A'_2 - A''_2} = \frac{1 + A''_2/A'_2}{1 - A''_2/A'_2} = \frac{1 + \sqrt{R}}{1 - \sqrt{R}} = Z$$

then $$R = \left| \frac{Z-1}{Z+1} \right|^2 \qquad \text{(A-11)}$$

All quantities on the right hand side of Equation (A-11) are physical properties of the sediment or water and Z is a complex number.

Formulating a_1 and b_1 as complex numbers gives the following:

$$a_1^2 = \frac{\rho_1 \left(\frac{c_w}{\sin \theta_i}\right)^2}{(\lambda'_1 - i\lambda''_1) + 2(\mu'_1 - i\mu''_1)} = H + jJ \qquad \text{(A-12)}$$

H and J are defined as follows:

$$H = \frac{\rho_1 \left(\frac{c_w}{\sin \theta_i}\right)^2 (\lambda'_1 + 2\mu'_1)}{(\lambda'_1 + 2\mu'_1)^2 + (\lambda''_1 + 2\mu''_1)^2} - 1 \qquad \text{(A-13)}$$

$$J = \frac{\rho_1 \left(\frac{c_w}{\sin \theta_i}\right)^2 (\lambda''_1 + 2\mu''_1)}{(\lambda'_1 + 2\mu'_1) + (\lambda''_1 + 2\mu''_1)^2} \qquad \text{(A-14)}$$

$$b_1^2 = \frac{\rho_1 \left(\frac{c_w}{\sin \theta_i}\right)^2}{\mu'_1 - i\mu''_1} - 1 = F + iG \qquad \text{(A-15)}$$

F and G are defined as follows:

$$F = \frac{\rho_1 \mu'_1 \left(\frac{c_w}{\sin \theta_i}\right)^2}{(\mu'_1)^2 + (\mu''_1)^2} - 1 \qquad \text{(A-16)}$$

$$G = \frac{\rho_1 \mu''_1 \left(\frac{c_w}{\sin \theta_i}\right)^2}{(\mu'_1)^2 + (\mu''_1)^2}$$

At this point the two Lamé constants λ'_1 and λ''_1 are contained only in the terms H and J. Equations (A-13) and (A-14) are then restated in terms of x and y as defined earlier in Equations (A-2) and (A-3).

$$H = \frac{\rho_1 x \left(\frac{c_w}{\sin \theta_i}\right)^2}{x^2 + y^2} - 1 = \frac{\rho_1 x\, c^2}{r^2} - 1$$

$$J = \frac{\rho_1 y \left(\frac{c_w}{\sin \theta_i}\right)^2}{x^2 + y^2} = \frac{\rho_1 y\, c^2}{r^2}$$

$$J = \rho_1 c^2 \left(\frac{x}{r^2}\right)\left(\frac{y}{x}\right) = \left(\frac{y}{x}\right)(H + 1)$$

Substituting from Equations (A-7) and (A-8) then yields the final expressions for H and J.

$$H = \left[\rho_1 \left(\frac{c_w}{\sin \theta_i}\right)^2\right]\left[\frac{1}{c_1^2} - \frac{1}{4}\left(\frac{a_p}{\pi f}\right)^2\right] - 1 \qquad \text{(A-18)}$$

$$J = \left[\frac{\left(\frac{c_1 a_p}{\pi f}\right)}{1 - \left(\frac{c_1 a_p}{2\pi f}\right)^2}\right]\left(H + 1\right) \qquad \text{(A-19)}$$

BIBLIOGRAPHY

1. White, J. E., Seismic Waves, McGraw-Hill, 1965, 302 p.

2. Hamilton, E. L., Naval Undersea Research and Development Center Report NUC TP 143, 144, 145, Sound Velocity, Elasticity and Related Properties of Marine Sediments, North Pacific, (three volumes), 1969.

3. Bucker, H. P., Whitney, J. A., Yee, G. S., and Gardner, R. R., "Reflection of Low-Frequency Sonar Signals from a Smooth Ocean Bottom," Journal of the Acoustical Society of America, v. 37, no. 6, p. 1037-1051, 1965.

4. Cohen, R. S., Measurement of the Viscoelastic Properties of Water-Saturated Clay Sediments, M. S. Thesis, Naval Postgraduate School, 1968, 60 p.

5. Martinek, C. A., Compressional Wave Speed and Absorption Measurements in a Saturated Kaolinite-Water Artifical Sediment, M. S. Thesis, Naval Postgraduate School, 1972, 40 p.

6. Borcherdt, R. D., Inhomogeneous Body and Surface Plane Waves in a Generalized Viscoelastic Half-Space, p. 1-26, Ph.D. Thesis, University of California, Berkeley, 1971, 308 p.

7. Kinsler, L. E. and Frey, A. R., Fundamentals of Acoustics, 2d ed., John Wiley & Sons, 1962, 466 p.

8. Morris, H. E., Naval Undersea Center Report NUC TP 327, Comparison of Calculated and Experimental Bottom-Reflection Losses in the North Pacific, 1972, 27 p.

9. Brekhovskikh, L. M., Waves in Layered Media, Academic Press, 1960, 561 p.

INITIAL DISTRIBUTION LIST

		No. Copies
1.	Defense Documentation Center Cameron Station Alexandria, Virginia 22314	2
2.	Library, Code 0212 Naval Postgraduate School Monterey, California 93940	2
3.	Professor O. B. Wilson, Jr., Code 61Wl Department of Physics Naval Postgraduate School Monterey, California 93940	5
4.	Professor R. S. Andrews, Code 58Ad Department of Oceanography Naval Postgraduate School Monterey, California 93940	5
5.	Department of Oceanography, Code 58 Naval Postgraduate School Monterey, California 93940	1
6.	Office of Naval Research Code 480D Arlington, Virginia 22217	1
7.	Oceanographer of the Navy Hoffman Building No. 2 2461 Eisenhower Avenue Alexandria, Virginia 22314	1
8.	Dr. William R. Bryant Texas A&M University Department of Oceanography College Station, Texas 77843	1
9.	Dr. Davis A. Fahlquist Texas A&M University Department of Geophysics College Station, Texas 77843	1
10.	Dr. E. L. Hamilton Naval Undersea Research and Development Center San Diego, California 92152	1

11. Commander R. M. Wellborn, Jr., USN — 1
25250 Outlook Drive
Carmel, California 93921

12. Dr. Robert E. Stevenson — 1
Scientific Liaison Office
Scripps Institution of Oceanography
La Jolla, California 92037

13. Mr. Homa Lee — 1
Naval Civil Engineering Laboratory
Port Hueneume, California 93041

14. Library — 1
U. S. Naval Oceanographic Office
Washington, D. C. 20390

15. Dr. H. P. Bucker — 1
Naval Undersea Research and Development Center
San Diego, California 92152

16. Mr. Tunkay Akal — 1
NATO SACLANT ASW Research Center
La Spezia, Italy

SECURITY CLASSIFICATION OF THIS PAGE *(When Data Entered)*

REPORT DOCUMENTATION PAGE

READ INSTRUCTIONS BEFORE COMPLETING FORM

1. REPORT NUMBER

2. GOVT ACCESSION NO.

3. RECIPIENT'S CATALOG NUMBER

4. TITLE *(and Subtitle)*

A Comparison of Measured and Calculated Acoustic Reflection Coefficients for a Saturated Kaolin-Water Artificial Sediment

5. TYPE OF REPORT & PERIOD COVERED
Master's Thesis
December 1973

6. PERFORMING ORG. REPORT NUMBER

7. AUTHOR(s)

Robert Morgan Wellborn, Jr.

8. CONTRACT OR GRANT NUMBER(s)

9. PERFORMING ORGANIZATION NAME AND ADDRESS

Naval Postgraduate School
Monterey, California 93940

10. PROGRAM ELEMENT, PROJECT, TASK AREA & WORK UNIT NUMBERS

11. CONTROLLING OFFICE NAME AND ADDRESS

Naval Postgraduate School
Monterey, California 93940

12. REPORT DATE
December 1973

13. NUMBER OF PAGES
50

14. MONITORING AGENCY NAME & ADDRESS *(if different from Controlling Office)*

Naval Postgraduate School
Monterey, California 93940

15. SECURITY CLASS. *(of this report)*
Unclassified

15a. DECLASSIFICATION/DOWNGRADING SCHEDULE

16. DISTRIBUTION STATEMENT *(of this Report)*

Approved for public release; distribution unlimited.

17. DISTRIBUTION STATEMENT *(of the abstract entered in Block 20, if different from Report)*

18. SUPPLEMENTARY NOTES

19. KEY WORDS *(Continue on reverse side if necessary and identify by block number)*

Kaolin
Reflection coefficient
Viscoelastic properties
Artificial sediments
Layered media reflection model
Bottom loss experiment
Reflection model

20. ABSTRACT *(Continue on reverse side if necessary and identify by block number)*

An acoustic energy reflection experiment was conducted in a laboratory tank containing water and an artificial kaolin sediment. The reflection coefficient for the sediment was measured for a limited range of angles of incidence at one frequency and one set of measured sediment mass physical and viscoelastic properties. A mathematical reflection model was derived in terms of the known sediment properties. The measured and the theoretically calculated reflection coefficients are compared. The measured reflection

DD FORM 1 JAN 73 1473 (Page 1)

EDITION OF 1 NOV 65 IS OBSOLETE
S/N 0102-014-6601

SECURITY CLASSIFICATION OF THIS PAGE *(When Data Entered)*

coefficient and a probable angle of intromission showed poor agreement with theoretically predicted values. For the sediment parameters of the relatively soft clay used here, the reflection model is quite sensitive to values of sediment density and sound speed and is only mildly sensitive to values of dynamic rigidity and sound absorption coefficient near the angle of intromission.

Thesis
W417
c.1
Wellborn
A comparison of measured and calculated acoustic reflection coefficients for a saturated kaolin-water artificial sediment.